ORIGINAL RESEARCH ARTICLE

Effect of Undercooling on the Microstructure and Mechanical Properties of Hyper-eutectic Ni–Sn Alloy

AHMED MUNAWAR, SADEEDA,VARDA ASIF, ALI JAFRI, FATIMA NISAR, MAREIKE WEGENER, JING SU, and FLORIAN KARGL

In this study, container-less solidification of hyper-eutectic Ni–Sn alloy has been performed by using the electromagnetic levitation technique. The effect of undercooling on the formed microstructure and on the mechanical properties have been investigated. Growth velocities were determined by high-speed video-imaging of the solidification process. A step change in the growth velocities that are increasing with increasing undercooling is observed. This aligns with an observed first change in the microstructure between low and intermediate undercoolings. At the lower undercoolings, a pro-eutectic Ni_3Sn phase along with lamellar eutectic structure in the inter-dendritic region is found. At intermediate undercooling of 100–150 K, a divorced eutectic microstructure is observed whereas at undercoolings above 165 K α-Ni precipitates are observed within β-Ni_3Sn dendrites. Microhardness testing revealed higher strength for the lamellar phase as compared to the non-lamellar phase. Nano-indentation has been performed to determine the hardness and strength of individual phases in the microstructure.

https://doi.org/10.1007/s11661-023-07172-z

I. INTRODUCTION

EUTECTIC and near-eutectic alloys are important for industrial applications because of their narrow temperature range and lower melting point than the pure elements.[1–3] A lot of studies have been performed to understand the solidification characteristics of undercooled eutectic systems *e.g.* Pb–Sn, Co–Si, Al–Si, Ni–Sn and Co–Mo.[2,4–8] As solidification velocity increases with increasing undercooling, lesser time is available for elemental diffusion, resulting in morphological changes. In several eutectic alloys, a morphological transition from a regular lamellar to an anomalous eutectic phase has been observed at larger undercooling as the regular lamellar eutectic phase cannot grow beyond a certain growth velocity.[2,9,10] A lower limiting value of undercooling where the anomalous eutectic phase starts to form was identified as well as a higher limiting value of undercooling at which the anomalous eutectic phase completely replaces the lamellar eutectic one. In between the two critical undercooling values (ΔT_{C1} and ΔT_{C2}), the microstructure consists of both lamellar and anomalous eutectic phases while the volume fraction of anomalous eutectic phase increases with rising undercooling.[2,11] Several mechanisms have been proposed for the formation of the anomalous eutectic phase. They include decomposition of a supersaturated solid solution,[9] cooperative or uncoupled dendritic growth of two phases[12,13] and re-melting of the fine lamellar eutectic phase.[11] For the eutectic Ni–Sn alloy, a dual mechanism has been mentioned which is responsible for the formation of anomalous eutectic formation.[11] This includes partial re-melting of eutectic dendrites and subsequent recrystallization of the Ni_3Sn matrix to form a fine-grained anomalous eutectic phase.[11] Similar findings have been reported in more recent studies involving Ni–Sn compositions.[14,15] A re-melting of even a few seconds is sufficient to convert the thermodynamically stable lamellar eutectic into fine- grained anomalous eutectic.[15] Re-melting of fine lamellar eutectics has also been proposed for the CoCrFeNiMnPd$_x$ eutectic high entropy alloy which results in the formation of a coarse granular eutectic phase.[16]

AHMED MUNAWAR is with the School of Chemical and Materials Engineering, National University of Sciences and Technology, 44000 Islamabad, Pakistan and also with the Institute of Materials Physics in Space, German Aerospace Center (DLR), Linder Höhe, 51170 Cologne, Germany. Contact e-mail: ahmed.munawar@duravit.de SADEEDA, VARDA ASIF, ALI JAFRI, and FATIMA NISAR are with the School of Chemical and Materials Engineering, National University of Sciences and Technology, 44000 Islamabad, Pakistan. MAREIKE WEGENER and FLORIAN KARGL are with the Institute of Materials Physics in Space, German Aerospace Center (DLR), Linder Höhe, 51170 Cologne, Germany. JING SU is with the Max-Planck Institute for Iron Research, Max-Planck-Straße 1, 40237 Düsseldorf, Germany.
Manuscript submitted October 2, 2022; accepted August 10, 2023.

Published online: 23 August 2023

There is plenty of literature available on the non-equilibrium solidification of hypo-eutectic and eutectic compositions of the Ni–Sn system,[9,11–13,17–19] however, most of the studies relate the effect of undercooling to the microstructure only. The present study is one of the very few dealing with the non- equilibrium solidification of hyper-eutectic Ni–Sn system and establishing a correlation between undercooling prior to solidification with the microstructure and the resulting mechanical properties.

Melt undercooling prior to solidification affects the crystal growth velocities in different ways.[2,4,5,8,20] For the Co-37.6pctMo eutectic alloy, the lower boundary of the coupled zone is 64 K below the eutectic point.[7] This is why "lamellar-nomalous eutectic" microstructural transition takes place at a critical undercooling of around 60 K.[7] For the Pb–Sn eutectic alloy, an undercooling of around 35 K results in the formation of anomalous eutectic with primary Pb dendrites instead of the usual lamellar eutectic with primary Pb dendrites.[5] For the eutectic composition of Ni–Sn alloy (Ni-18.7 at.pct Sn), the sudden increase in crystal growth velocity is observed at undercoolings above 160 K where the transition of crystal growth mode from sluggish coupled growth of eutectic dendrites to rapid uncoupled growth of single-phase Ni-rich dendrites takes place.[11] Crystal growth velocities not only affect the final microstructure but also the resulting mechanical properties. In case of Fe-based alloys, rapid dendrite growth results in improved mechanical properties. This is due to the grain refinement, the homogeneous distribution of the Fe_7Mo_3 phase along the boundaries and increased multi-solute contents inside the grain. The increase in microhardness is rapid with increasing undercooling, however, it slows down at larger undercoolings due to the microstructural transition from a trunk-dendrite to an equi-axed grain microstructure.[21] .For Fe–Ni, Vickers microhardness exhibits a well-defined Hall–Petch slope as a function of grain size.[20] Validation of Hall–Petch relation has also been observed for rapidly solidified eutectic alloys, where the hardness increases as the lamellar spacing decreases due to the reduced solidification time.[22,23] Such a correlation has not been developed yet for lamellar and anomalous eutectics as a function of undercooling. The present study focuses on elucidating the relationship between undercooling and mechanical properties of hyper-eutectic Ni–Sn alloy. The micromechanical properties have been determined using Vickers microhardness test while nano-indentation has been performed to observe the local mechanical property variations of the solidified phases.

II. EXPERIMENTAL PROCEDURE

Hyper-eutectic samples of $Ni_{79.3}Sn_{20.7}$ have been prepared by arc melting together Ni and Sn of 99.999 pct purity under Ar-protected atmosphere with argon purity of 99.999 pct. All the samples had a mass of around 1.0 g while the mass loss during arc melting was in the range of 0.001 g. The samples were processed by electromagnetic levitation (EML). Cooling of the samples was done by using a He gas flow in the same EML set up. During the heating and cooling cycle, the temperature was measured using a single-color pyrometer. A high-speed camera, capturing 10000 frames/s was utilised to observe the recalescence process. After the samples were solidified, they were prepared by metallographic techniques to be investigated using optical and scanning electron microscopy (SEM). A LEO 1530VP microscope by Zeiss equipped with backscatter detector (BSD) and energy-dispersive X-ray analysis (EDX) system Inca by Oxford Instruments has been used for this purpose.

The Vickers microhardness of the undercooled samples was measured using Wolpert Microhardness tester. The applied load was 500 gF and the dwell time was kept constant at 15 seconds for all the tests. The machine was calibrated on regular basis during the testing of samples to ensure that the instrumental error is less than 1 pct. After the load was removed, two of the impression diagonals were measured with a micro-meter eyepiece and the calculation of microhardness is based on the length of the diagonal. The distance between two adjacent indents was kept more than three times the diagonal length of an indentation. At least 10 indents were made on each sample from the periphery towards the centre. Optical microscopy was performed to identify the location of each indent and to investigate the micro-hardness of lamellar and non-lamellar phases.

Nanoindentation tests were performed using a Hysitron Tribo indenter TI900 system with an applied load of 2000 μN under load control mode. A diamond Berkovich probe, which is a three-sided pyramidal probe with a curvature radius of 50nm, an included angle of 142.35 deg and a half angle of 65.35 deg was adopted for the test. The Berkovich tip was calibrated using a standard fused quartz sample and a trapezoid load function.

III. RESULTS AND DISCUSSION

A. *Cooling Curves*

A series of undercoolings, ranging from 10 to 205 K, have been achieved for hyper-eutectic Ni–Sn samples in this study. Figure 1 shows a representative cooling curve of a sample which has shown an undercooling of around 125 K prior to solidification.

As the sample is heated up from room temperature, it undergoes a solid-solid transformation at 1220 K from low temperature Ni_3Sn hexagonal phase to high temperature Ni_3Sn cubic phase. As the temperature is further increased, the sample undergoes melting at around 1420 K which is the liquidus temperature on the phase diagram. The temperature remains constant till the entire sample is molten. The sample is then superheated for some time at higher temperature before it is cooled down. Due to the container-less nature of the solidification process, the sample does not solidify at the equilibrium melting point. Instead, it can be significantly undercooled below its liquidus before the solidification

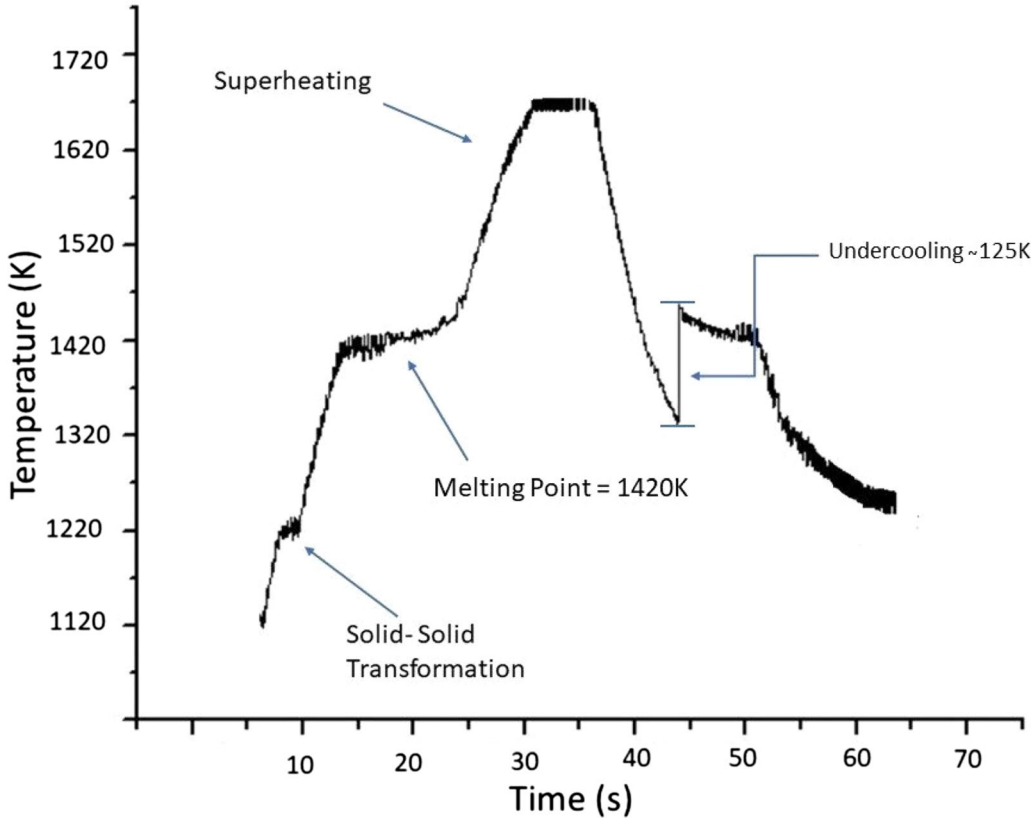

Fig. 1—Cooling curve showing a typical melting-solidification cycle as observed in EML-experiments on Ni–Sn20.7 at.pct samples. In the present experiment an undercooling of around 90K was reached.

process starts, depicted by a sharp increase in temperature due to recalescence. The portion of sample solidified during the recalescence phase is directly proportional to the undercooling prior to solidification. After a portion has been solidified during the recalescence phase, the remaining solidification takes place over a narrow melting temperature range. As soon as the whole sample solidifies, the temperature goes down further. At room temperature, the Ni_3Sn exists as the low temperature hexagonal phase.

Near-equilibrium solidification of the Ni-20.7 at.pct Sn hyper-eutectic alloy starts with the primary formation of the pro-eutectic β-Ni_3Sn phase with substantial solubility of Ni. As the β-Ni_3Sn phase grows, this phase but also the remaining liquid decreases in Sn content. At 1412 K, the remaining liquid has exactly the eutectic composition of 18.7 at.pct Sn which then solidifies forming a lamellar eutectic microstructure consisting of α-Ni and β-Ni_3Sn. In the present study, the sample undergoes large values of undercooling prior to solidification and consequently the formation and growth of non-equilibrium microstructures are expected which will be discussed in the upcoming sections.

B. *Recalescence Behaviour and Crystal Growth Velocities*

High speed video images of the solidification process are shown in Figure 2. The top figure was taken at an undercooling of 20 °C undercooling. In the present study, a single nucleation event for the entire solidification has been observed for each of the samples where the recalescence front sweeps around and through the entire sample. At low undercooling, the front has a nearly circular shape with no special features. At larger undercooling, the front shows edges especially at the beginning of solidification. The appearance of such edges in the solidification front on the sample's surface indicates an underlying network of co-operatively growing dendrites.[24]

As a single nucleation event has been recorded for all the samples in this study. No double recalescence or copious nucleation was observed for the solidification event, as it has been the case in a previous study.[25] The crystal growth velocity for the solidification front was determined using first-frame-last-frame method analysing the recorded high-speed video-images. Figure 3 shows the relationship between the crystal growth velocity and undercooling. At lower undercoolings, the increase in solidification velocity with respect to undercooling is moderate. However, after reaching a certain critical undercooling range (90–110 K) higher crystal growth velocities and a different dependence with undercooling are observed. In addition, the scatter in the velocity data is larger.

C. *Microstructural Evolution*

The microstructures of hyper-eutectic Ni–Sn alloy solidified at different undercoolings prior to solidification are shown in Figures 4(a) through (c). The sample solidified at an undercooling of 20 K shows pro-eutectic

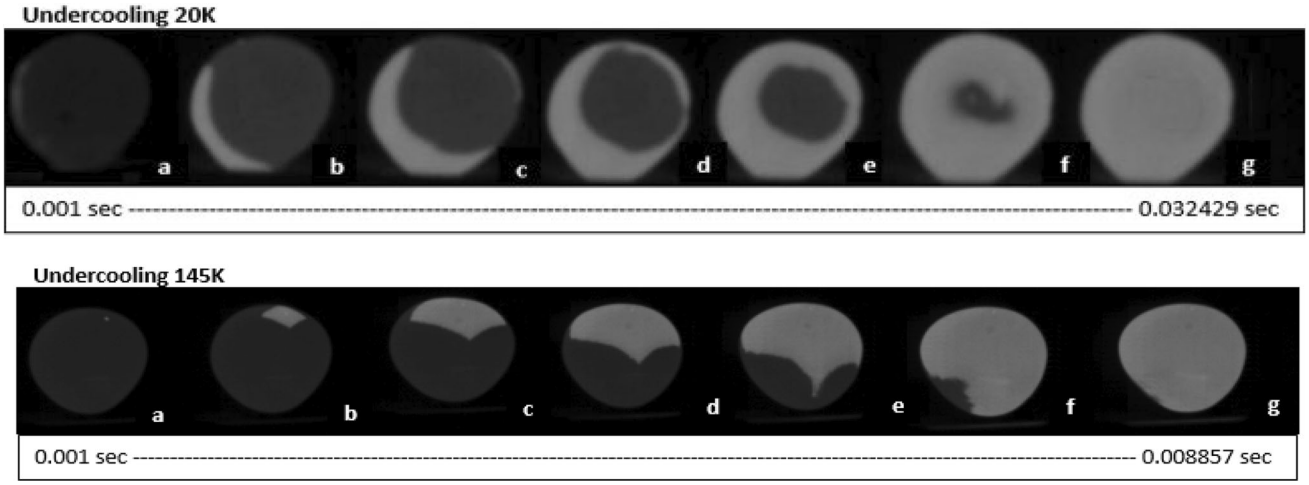

Fig. 2—High speed video camera images of solidification fronts, above) undercoolings of 20 K and below) undercooling of 145 K.

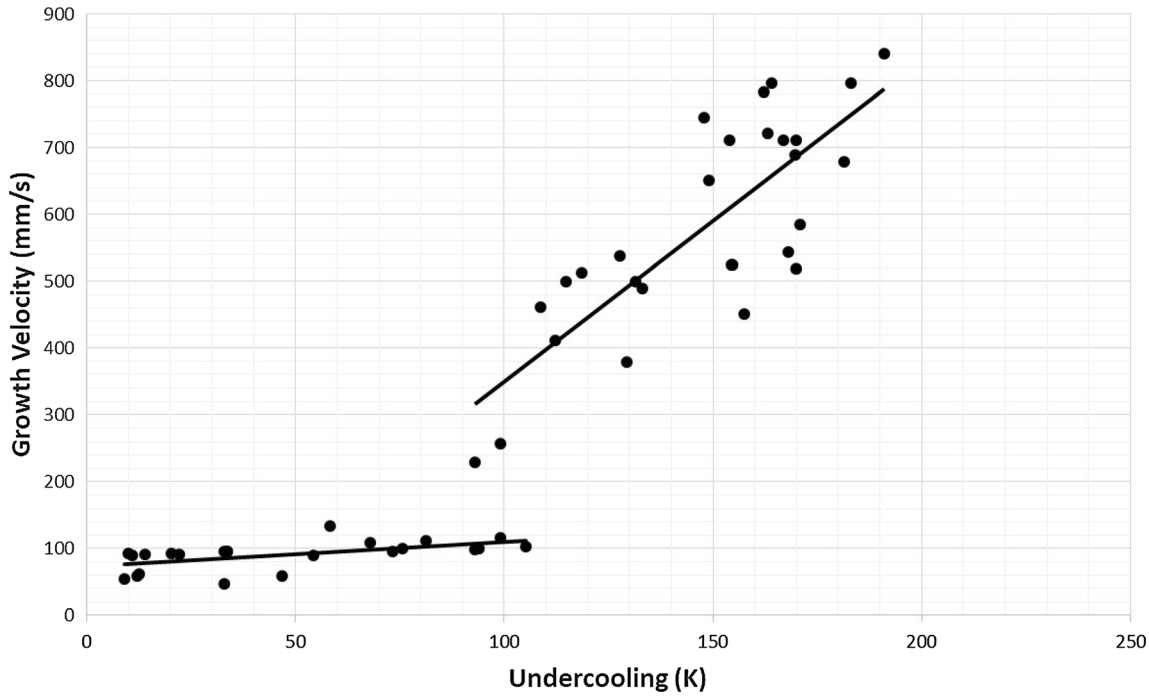

Fig. 3—Crystal growth velocity vs undercooling for the hyper-eutectic Ni-20.7 at.pct Sn alloy solidified using electro-magnetic levitation.

β-Ni_3Sn dendrites and a lamellar eutectic phase consisting of the α-Ni phase (dark) and the β-Ni_3Sn (light grey) intermetallic compound [Figure 4(a)]. On the surface of the sample, a ~ 10 μm thin layer of β-Ni_3Sn is found. As the undercooling increases, the solidification process becomes more rapid and consequently there is not enough time available for the formation of lamellar eutectic. The microstructure of such a sample solidified with an undercooling of 145 K is shown in the Figure 4(b). The microstructure consists of β-Ni_3Sn dendrites while the α-Ni appears to be segregated out. This is more visible in the regions close to the surface of the sample. Towards the middle of this sample, the microstructure is similar to the one shown in Figure 4(a). It is because only a part of the sample is solidified at larger undercooling (''recalescence phase'') while the remaining part has been solidified in the temperature around the equilibrium melting range.

Figure 4(c) shows the microstructure obtained for the samples solidified at the highest undercoolings in this study. This microstructure, which is more evident towards the surface of the sample, consists of Ni_3Sn dendrites where the α-Ni appears to be precipitated out at several locations within the dendrites. For all the samples, at least some lamellar eutectic has been found towards the centre which is the last part to be solidified in this study.

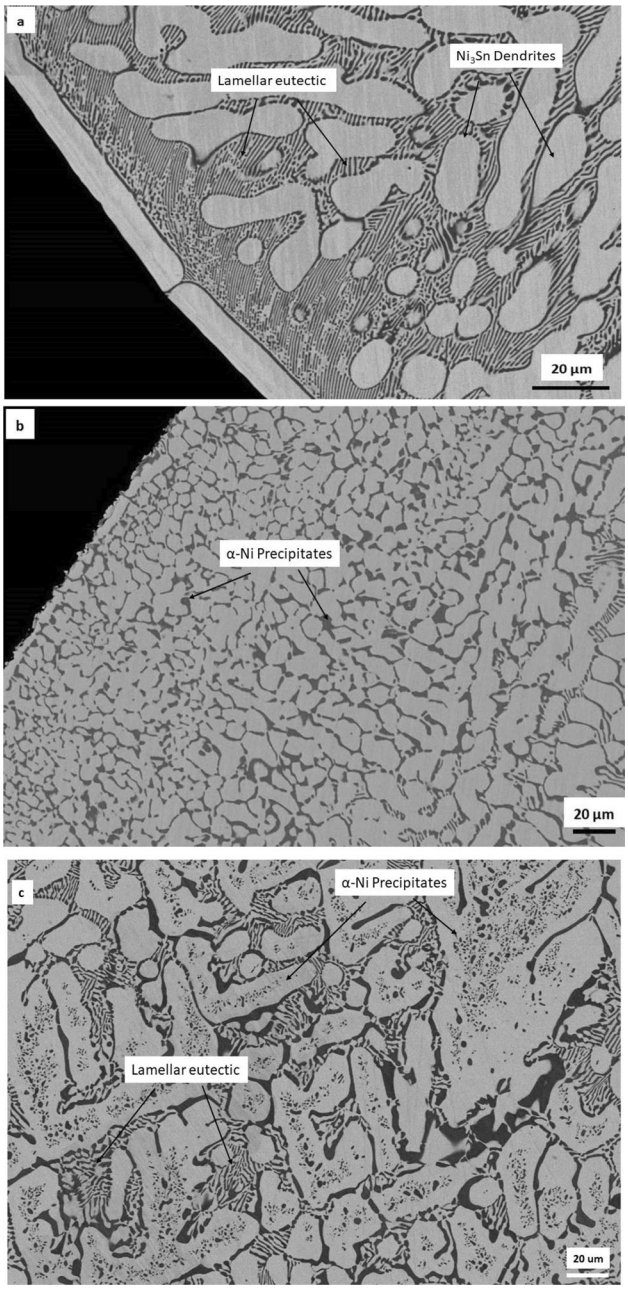

Fig. 4—Microstructure of hyper-eutectic Ni–Sn sample solidified at (*a*) 20 K, (*b*) 145 K and (*c*) 175 K undercooling. The α-Ni phase appears dark while the *β*-Ni_3Sn appears bright in all SEM micrographs.

D. *Microhardness*

Microhardness of hyper-eutectic Ni–Sn alloy solidified at different undercooling has been investigated using Vickers microhardness equipment and the result is shown in Figure 5. The measurements were started at the periphery of the samples and then the indents were made towards the centre. This means the 1st measurement point in the Figure 5 is towards the periphery where the solidification is usually the fastest while the last measurement points are towards the centre where the solidification velocity is slower. The microhardness observed in the middle region is around 470 HV which corresponds to 4.6 GPa. Towards the periphery of samples where different microstructures have been observed at different undercoolings, the microhardness values are different. The samples solidified after undercooling of 165 and 172 K show microhardness in the range of 370 HV (3.62 GPa) at the periphery while the sample solidified at 20 K showed 405 HV (3.97 GPa). After performing the micro-indentation, the samples were investigated using optical microscope to find out the location of each indent. One such optical micrograph has been shown in the inset of Figure 5.

E. *Nano-indentation*

Nano-indentation was performed to determine the hardness of individual phases present in the microstructure. Two samples, solidified at different undercoolings, were chosen for the nano-indentation testing. More than 50 indents were made on both the samples to determine the hardness of different phases. After nano-indentation, SEM was performed using BSE detector to identify the location of each indent and correlate it with the hardness value. Nano indentation for the sample solidified at 165 K is shown in Figure 6 along with the hardness and elastic modulus. The nano-indents on Ni_3Sn phase have been encircled in red whereas the nano-indents on the α-Ni phase have been encircled in blue. The hardness of the α-Ni phase has been found to be in the range of 6–7 GPa while that of Ni_3Sn phase is in the range of 10 GPa. The lowest values have been achieved when the nano-indents lie completely on the α-Ni phase. The values of hardness obtained nano-indentation are higher than the ones shown by micro-hardness technique. This is due to the indentation size effect (ISE), which says that the crystalline materials often show depth-dependent hardness until the indentation depth is larger than 1 μm.[26–28] Below the indentation depth of 1μm, most crystalline materials show higher strength and hardness. As the depth of nano-indents in the current study is always below 100 nm, the measured values of hardness are in accordance with the above-mentioned indentation size effect.

IV. DISCUSSION

In the present study, single nucleation events have been recorded in the solidification of all the samples. In contrary to the case of multiple nucleation events, this allows to determine crystal growth velocity as a function of undercooling. The crystal growth velocity has been calculated by measuring the time between the start and the end of solidification and dividing it by the diameter of the sample. High speed camera recording the solidification event at 10000 frames per second has been used to determine the start and completion of the solidification. Figure 2 shows that the increase in crystal growth velocity w.r.t increasing undercooling is small at lower undercooling values. However, at undercooling larger than 100–120 K, the increase in crystal growth velocity becomes rapid. The reason for the sudden increase in

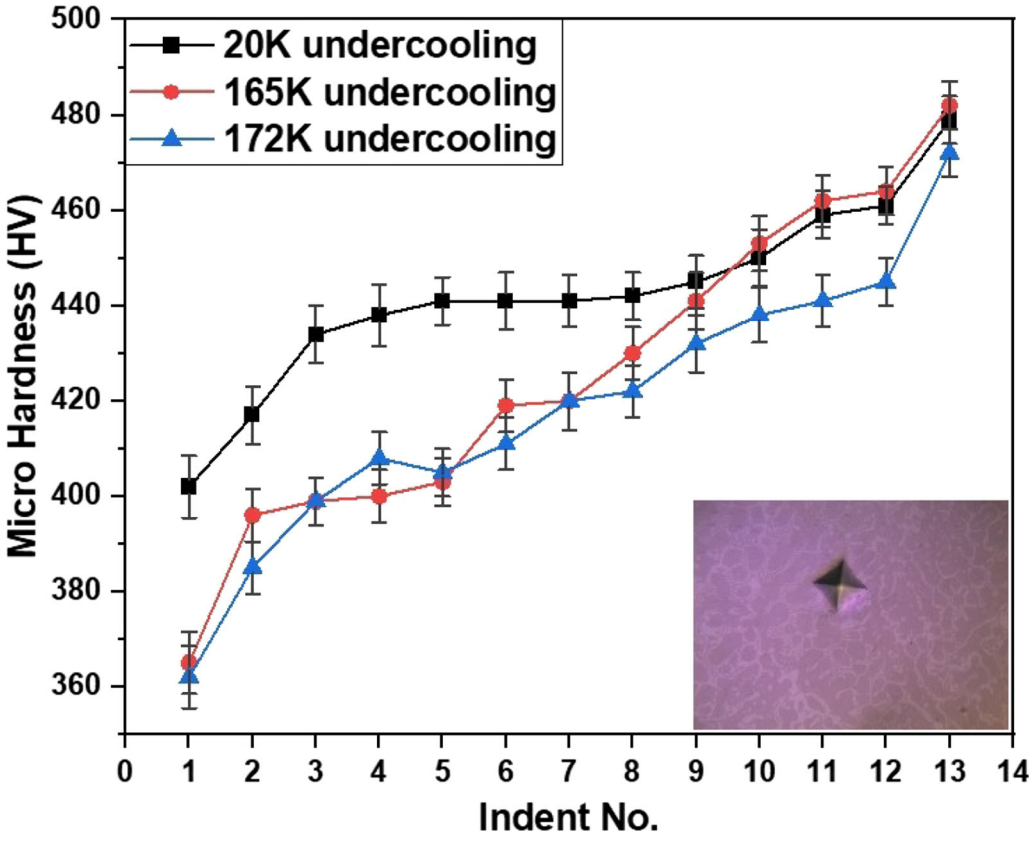

Fig. 5—Microhardness values of hyper-eutectic Ni–Sn samples solidified at different undercoolings. An optical micrograph with a micro-indent is shown in the inset.

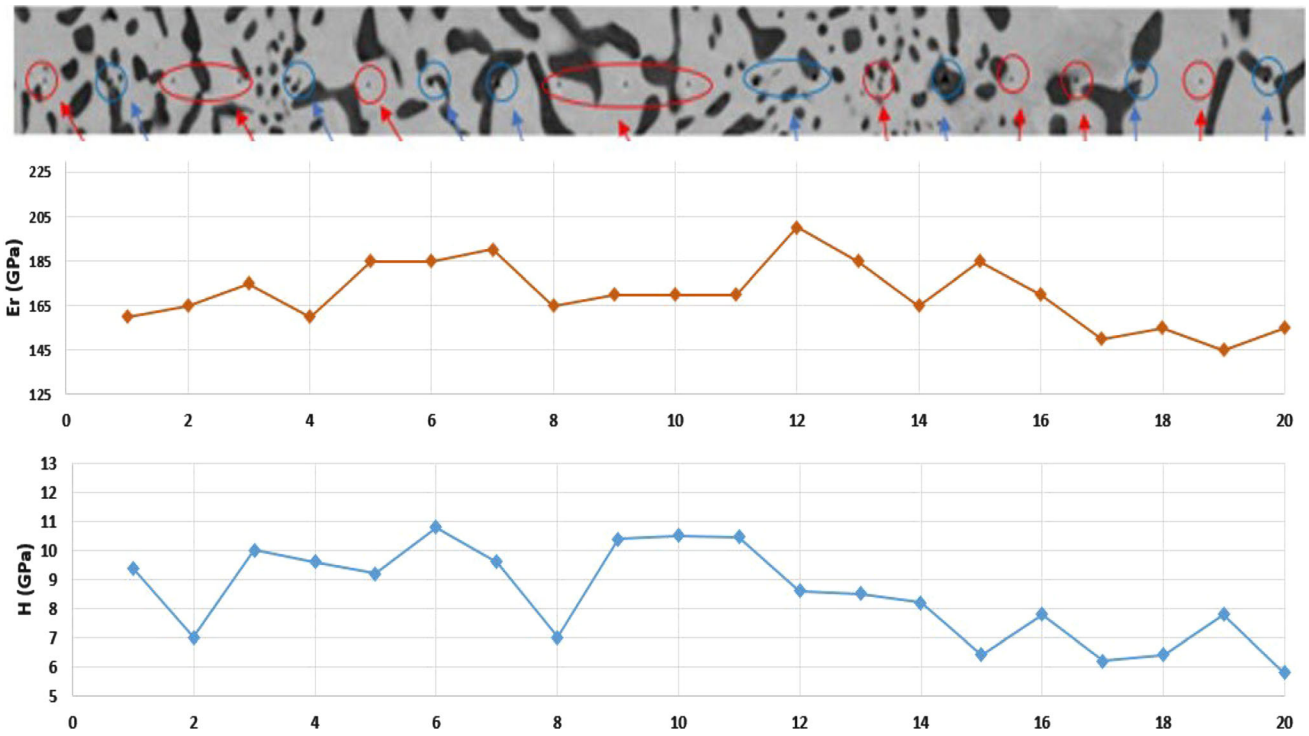

Fig. 6—Nano-mechanical properties of the hyper-eutectic Ni–Sn alloy solidified at 165 K undercooling.

crystal growth velocity in Ni–Sn is usually attributed to the transition from coupled eutectic growth mode to the uncoupled growth of α-Ni phase and β-Ni_3Sn phases.[7,9,12,13,17,18] This seems to be the case in the present study as well where coupled growth took place at lower undercoolings resulting in a lamellar eutectic microstructure in the inter-dendritic region. At larger undercoolings, different microstructures have been observed which will be discussed below.

Two different microstructures have been observed at larger undercoolings, shown in Figures 4(b) and (c). The microstructure shown in Figure 4(b) is obtained at intermediate undercoolings ranging between 100 and 150K. It consists of a divorced eutectic structure of β-Ni_3Sn dendrites with α-Ni phase segregated at the inter-dendritic region. This clearly shows that the solidification velocity has been too fast to allow the formation of lamellar eutectic in this region. As a result, uncoupled growth of β-Ni_3Sn and α-Ni phases results in the microstructure shown in Figure 4(b). In addition to the uncoupled growth, divorced eutectics rarely incorporate the interactions between the two eutectic phases, as reported in a recent study.[29] In case of hypoeutectic and eutectic compositions of Ni–Sn, anomalous eutectic has been found to develop at larger undercooling values.[7,9,12,13,17,18] In the present study, the microstructure obtained for the largest undercoolings (*i.e.* above 165 K) is shown in Figure 4(c) where α-Ni precipitates could be seen within the β-Ni_3Sn dendrites. It is possible that due to large undercooling, the solidification begins at a temperature where eutectic dendrite forms in the beginning instead of the β-Ni_3Sn, which could then undergo re- melting. Similar re-melting of eutectic dendrites has also been speculated during the solidification of $CoCrFeNiMnPd_x$ eutectic high entropy alloy with higher Pd-content.[16] For the Ni–Sn system, it was proposed by Kattamis and Flemings that the first solid formed at very large undercooling was a highly supersaturated α-Ni solid solution of eutectic composition (Ni-18.7 at.pct Sn), which grew dendritically and later decomposed to the equilibrium α-Ni and β-Ni_3Sn during the post-recalescence.[9] In another study, three different eutectic systems have been studied and it has been concluded that partial re-melting takes place because of the supersaturation of solute.[20] In some recent studies involving different Ni–Sn compositions, remelting of eutectic dendrites has been reported resulting in non-equilibrium microstructures.[14,15] This seems to be the case in the present work as well where due to large undercooling; nucleation could start below the eutectic temperature resulting in the formation of eutectic dendrite instead of β-Ni_3Sn dendrite. However, due to the rapid increase in temperature during recalescence phase, partial re-melting takes place resulting in excess Ni precipitating out within the β-Ni_3Sn dendrites. In a recent study, non-equilibrium solidification of hyper-eutectic Nb–Si alloy has been performed using electrostatic levitation. A transition from the primary faceted Nb_3Si phase to the non-faceted Nb phase, and then to the complete eutectic has been observed with the increase of undercooling, however, no re-melting has been reported.[30]

Micro- and- nano-indentation has been carried out to investigate the mechanical behaviour changes as a function of undercooling. Nano-indents give the information about the mechanical properties while the micro-indents indicate the hardness due to microstructure as well. It can be seen in Figure 6, that the hardness of β-Ni_3Sn phase is higher than that of the α-Ni phase. This is mainly because of stronger bonding between the constituents of the intermetallic phase. Intermetallic compounds typically show properties in between those of ceramic and metals, namely having a high hardness, increased brittleness, and a higher melting point.[3] In Figure 6, the lowest hardness value is observed when the nano-indent lies completely on the α-Ni phase. The hardness values are slightly increased when the nano-indent lies on a phase boundary or close to it. The hardening effect of the grain or phase boundary is attributed to the well-known dislocation pile-up which takes place at the boundary. It is because the dislocations, which play the most important role in plastic deformation, experience more hindrance in movement due to grain boundaries. Consequently, fine grained structures tend to show higher strength due to more grain boundaries.[31,32] The effect of phase boundaries together with individual phase hardness is summed up in micro-hardness where the indent covers a larger area. It has been observed that the lamellar microstructure shows greater hardness as compared to the non-lamellar one which means that the micro-hardness decreases with increasing undercooling in this special alloy. This is in accordance with another study where eutectic high entropy alloy samples with lamellar microstructure showed better mechanical properties than the samples where spheroidization of lamellar structure had taken place.[33] For the Nb–Si alloy, a similar trend has been observed where the Vickers hardness is the highest for the master alloy while lower hardness has been observed for the samples solidified at larger undercoolings.[30] In another study involving Fe-based multinary alloy, the effect of undercooling on mechanical properties has been investigated.[21] It has been reported that rapid dendritic growth of Fe-based multinary alloy leads to grain refinement resulting in the formation of equi-axed grains which have higher hardness. The hardness change has been attributed to the combined effect of grain refinement, 2nd phase formation and solute entrapment. In the present study, no new phase has been formed even at the largest undercooling and solute entrapment has not been observed. The decrease in micro-hardness at larger undercoolings is attributed to the formation of non-lamellar microstructure.

V. CONCLUSION

Hyper-eutectic Ni–Sn samples have been solidified at undercoolings up to 205 K using electro-magnetic levitation and the effect of undercooling on the solidification velocity, microstructure and mechanical properties have been investigated. The key results are summarized as below:

I Single primary nucleation events have been observed for all the solidifying samples where the recalescence front sweeps through or around the entire sample from one side to the other. As a result, it is possible to determine the crystal growth velocities as a function of undercooling.

II The measured crystal growth velocities at low undercoolings increase moderately with increasing undercooling. However, above 120 K, a rapid increase in growth velocities has been observed. This phenomenon has been observed previously for Ni–Sn as well, where the transition from coupled crystal-growth to the un-coupled crystal-growth takes place around that temperature.

III Solidification of the Ni-20.7 at.pct Sn alloy with low undercooling values results in primary dendrites of pro-eutectic β-Ni_3Sn phase with an inter-dendritic lamellar eutectic phase of α-Ni and β-Ni_3Sn. With increasing undercooling, the solidification is much faster as to allow the formation of lamellar eutectic phase. As a result, the α-Ni phase appears to be segregated out of the β-Ni_3Sn dendrites forming a divorced eutectic microstructure. The samples solidified at the highest undercooling in this study showed precipitates of α-Ni within the β-Ni_3Sn phase which might be due to the re-melting of initially formed eutectic dendrite.

IV Nano indentation results revealed a greater hardness for the β-Ni_3Sn phase, as compared to the α-Ni. The value of nano-hardness increases when the indent is close to the phase boundary.

V Microhardness testing was performed using Vickers microhardness. The results showed that the samples solidified at lower undercoolings show greater microhardness as compared to the samples solidified at larger undercoolings. This difference is due to the lamellar phase which shows greater microhardness due to the presence of more phase boundaries.

CONFLICT OF INTEREST

The authors declare no conflict of interest.

FUNDING

Open Access funding enabled and organized by Projekt DEAL.

OPEN ACCESS

REFERENCES

1. D.M. Herlach: *Metals*, 2014, vol. 4(2), pp. 196–234.
2. D.M. Herlach and D.M. Matson: *Solidification of Containerless Undercooled Melts*, Wiley, New York, 2012.
3. D.A. Porter and K.E. Easterling: *Phase Transformations in Metals and Alloys*, CRC Press, Boca Raton, 2009.
4. W.B.C. de Castro: ML de Maia, CS Kiminami, C Bolfarini. *Mater. Sci. Eng. A*, 2001, vol. 304, pp. 255–61.
5. H. Kang and W. Yoon: *Mater. Trans.*, 2004, vol. 45, pp. 2956–59.
6. R.P. Liu, D. Herlach, M. Vandyoussefi, and A.L. Greer: *Metall. Mater. Trans. A.*, 2004, vol. 35(2), pp. 607–12.
7. B. Wei, D. Herlach, F. Sommer, and W. Kurz: *Mater. Sci. Eng. A*, 1994, vol. 181, pp. 1150–55.
8. W. Yao, N. Wang, and B. Wei: *Mater. Sci. Eng. A*, 2003, vol. 344(1–2), pp. 10–19.
9. T.Z. Kattamis and M.C. Flemings: *Metall. Mater. Trans. B.*, 1970, vol. 1, p. 1449.
10. J. Li, X. Li, L. Liu, and S. Lu: *J. Mater. Res.*, 2008, vol. 23(8), pp. 2139–48.
11. C. Yang, J. Gao, Y. Zhang, M. Kolbe, and D.M. Herlach: *Acta Mater.*, 2011, vol. 59(10), pp. 3915–26.
12. W. Bingbo, Y. Gencang, and Z. Yaohe: *Acta Metall. Mater.*, 1991, vol. 39(6), pp. 1249–58.
13. Y. Wu, T. Piccone, Y. Shiohara, and M. Flemings: *Metall. Trans. A*, 1988, vol. 19(4), pp. 1109–19.
14. H. Dong, Y. Chen, K. Wang, G. Shan, Z. Zhang, K. Huang, and F. Liu: *Scripta Mater.*, 2020, vol. 177, pp. 123–27.
15. R. Zhao, Y. Wang, J. Gao, E.B. Baker, D.M. Matson, M. Kolbe, A.C.-P. Chuang, and Y. Ren: *Acta Mater.*, 2020, vol. 197, pp. 198–211.
16. Y. Tan, J. Li, J. Wang, M. Kolbe, and H. Kou: *J. Alloys Compd.*, 2018, vol. 731, pp. 600–11.
17. Y. Wu, T. Piccone, Y. Shiohara, and M. Flemings: *Metall. Mater. Trans. A.*, 1987, vol. 18(5), pp. 915–24.
18. Y. Wu, T. Piccone, Y. Shiohara, and M. Flemings: *Metall. Mater. Trans. A.*, 1987, vol. 18(5), pp. 925–32.
19. L. Xing, D. Zhao, and X. Chen: *J. Mater. Sci.*, 1993, vol. 28(10), pp. 2733–37.
20. X. Wei, X. Lin, W. Xu, Q. Huang, M. Ferry, J. Li, and Y. Zhou: *Acta Mater.*, 2015, vol. 95, pp. 44–56.
21. Y. Ruan, A. Mohajerani, and M. Dao: *Sci. Rep.*, 2016, vol. 6(1), pp. 1–11.
22. U. Büyük, M. Erol, T. Volkmann, and D.M. Herlach: *Adv. Eng. Mater.*, 2015, vol. 17(3), pp. 359–65.
23. E. Çadırlı, D.M. Herlach, and T. Volkmann: *J. Non-Cryst. Solids*, 2010, vol. 356(9–10), pp. 461–66.
24. S. Binder, M. Kolbe, S. Klein, and D. Herlach: *Europhys. Lett.*, 2012, vol. 97, p. 36003.
25. M. Li, K. Nagashio, and K. Kuribayashi: *Acta Mater.*, 2002, vol. 50(12), pp. 3241–52.
26. K. Durst, B. Backes, O. Franke, and M. Göken: *Acta Mater.*, 2006, vol. 54(9), pp. 2547–55.
27. G.M. Pharr, E.G. Herbert, and Y. Gao: *Annu. Rev. Mater. Res.*, 2010, vol. 40, pp. 271–92.
28. J. Swadener, E. George, and G. Pharr: *J. Mech. Phys. Solids*, 2002, vol. 50(4), pp. 681–94.

29. J.-H. Kang, J. Park, K. Song, C.-S. Oh, O. Shchyglo, and I. Steinbach: *J. Magnes. Alloys*, 2022, vol. 10(6), pp. 1672–79.
30. M.X. Li, H.P. Wang, M.J. Lin, C.H. Zheng, and B. Wei: *Acta Mater.*, 2022, vol. 237, p. 89.
31. E. Hall: *Proc. Phys. Soc. Sect. B*, 1951, vol. 64(9), p. 747.
32. N.J. Petch: *J. Iron Steel Inst.*, 1953, vol. 174, pp. 25–28.
33. F. He, Z. Wang, X. Shang, C. Leng, J. Li, and J. Wang: *Mater. Des.*, 2016, vol. 104, pp. 259–64.